Supporting information:

Porous Co_9S_8/Nitrogen, Sulfur-Doped Carbon@Mo_2C Dual Catalyst for Efficient Water Splitting

Xiaohu Luo,[a,b] Qiulan Zhou,[a] Shuo Du,[a] Ji Li,[a] Jiawen Zhong,[a] Xiulin Deng,[a] and Yali Liu[a]*

[a] State Key Laboratory for Chemo/Biosensing and Chemometrics, College of Chemistry and Chemical Engineering, Hunan University, Changsha, Hunan, 410082, P. R. China

[b] School of Chemistry and Chemical Engineering, Qiannan Normal University for Nationalities, Duyun, Guizhou, 558000, P. R. China

* E-mail address of corresponding author: yaliliu@hnu.edu.cn

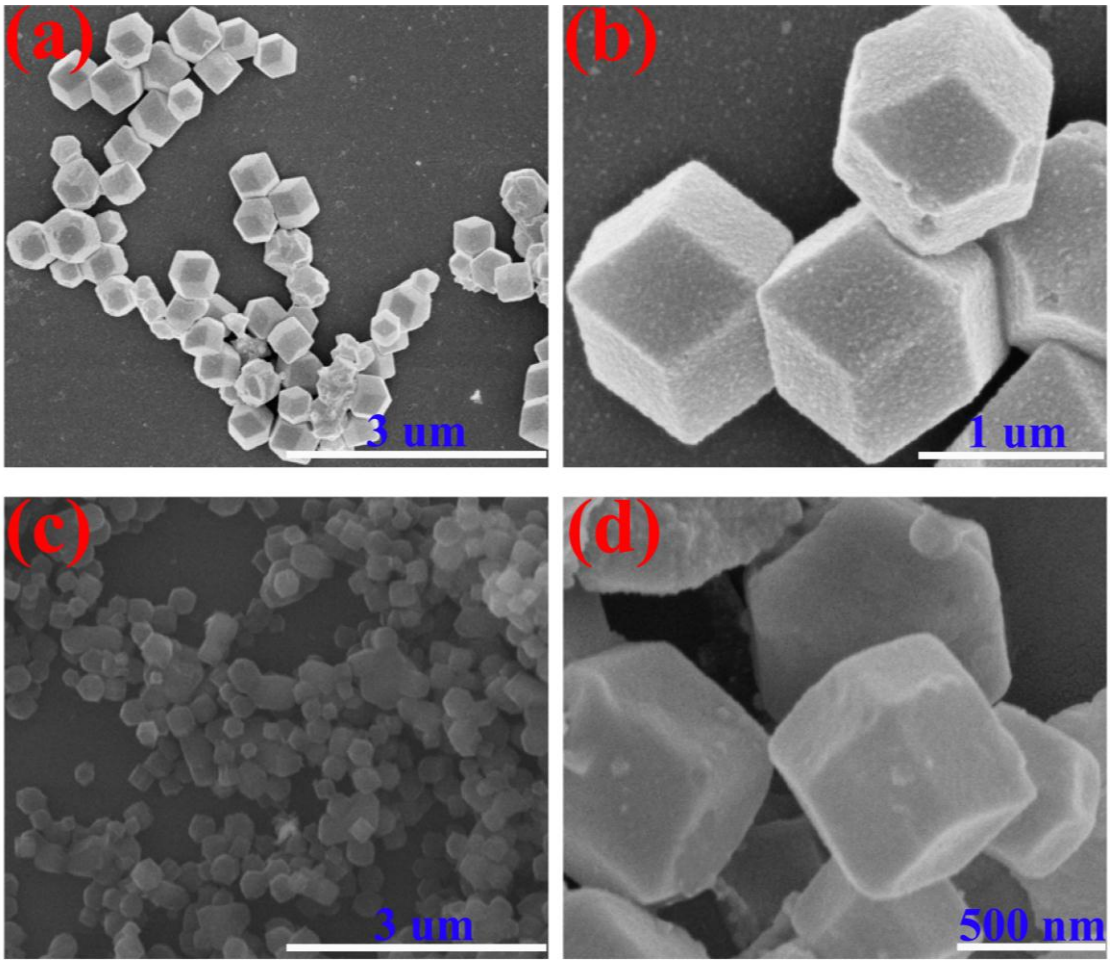

Figure S1. SEM images of the (a, b) Co-ZIF-67 and the (c, d) P-2AT@Co-ZIF-67.

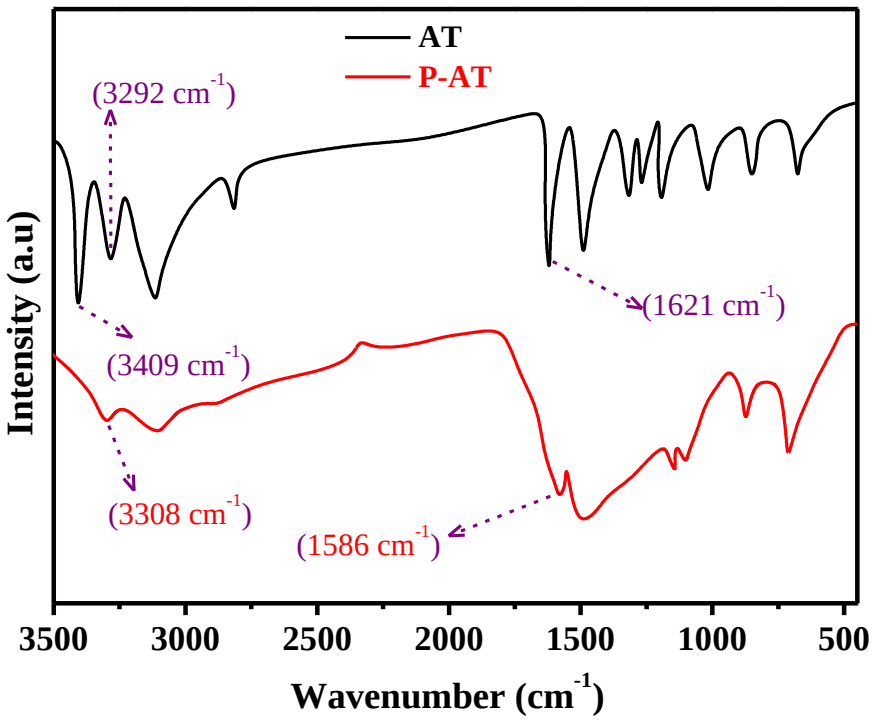

Figure S2. FT-IR spectra of AT and P-AT.

It can been seen in **Figure S**2 that the bands appeared at 3409 cm^{-1} and 3292 cm^{-1} are attributed to the asymmetrical and symmetrical N-H stretching of AT. However, a broad band of P-AT is at 3308 cm^{-1} is assigned to the N-H stretching, and the band of C=N stretching shifts from 1621 cm^{-1} to 1586 cm^{-1}.[S1] These results indicate the successful polymerization of AT.

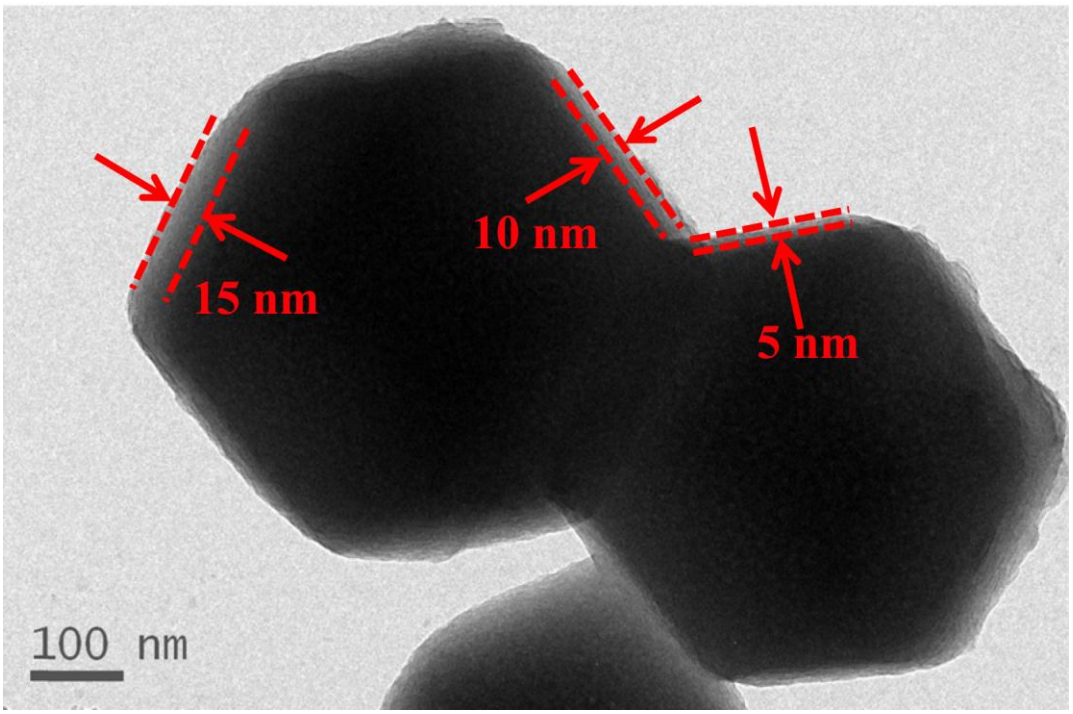

Figure S3. TEM images of P-TA@Co-ZIF-67.

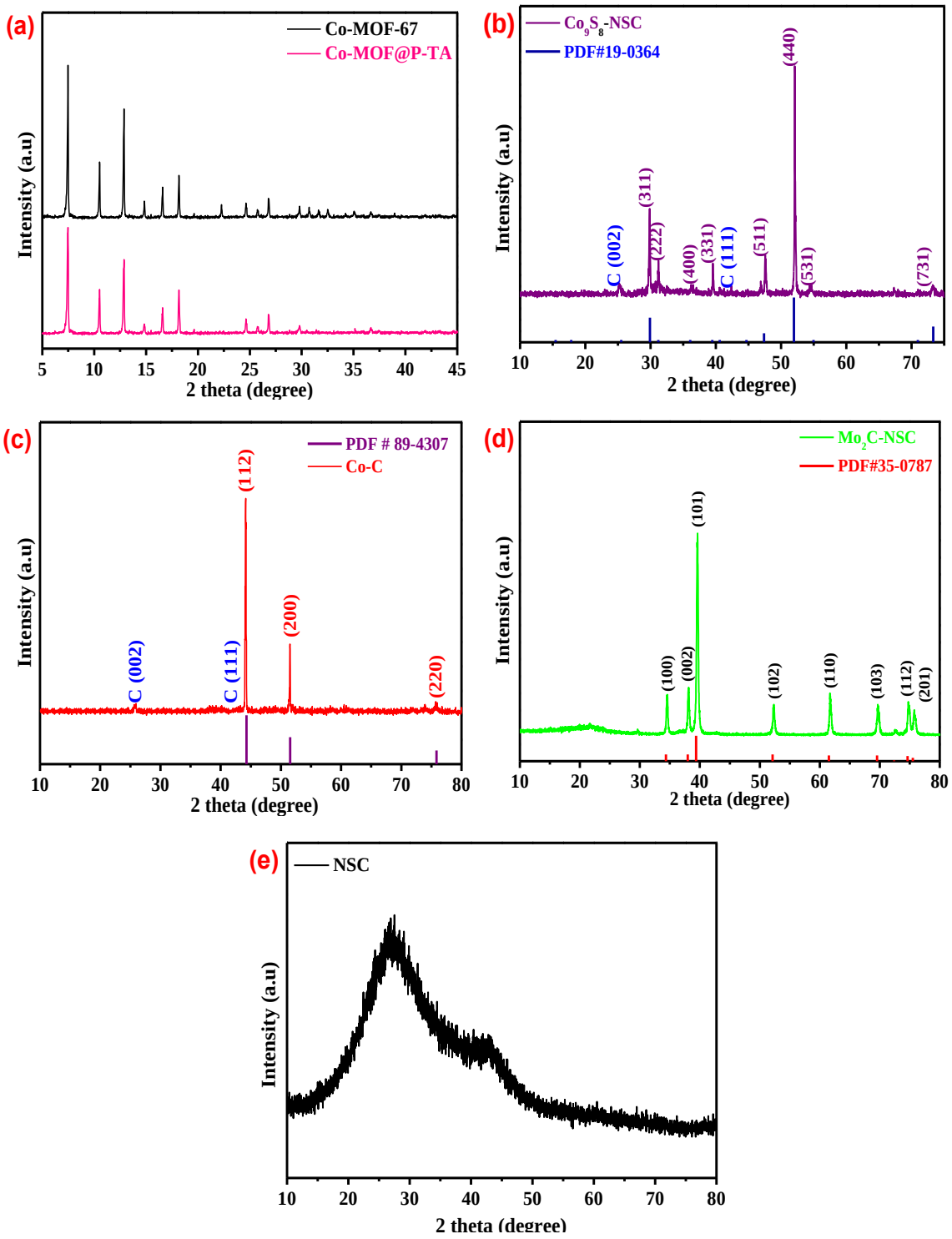

Figure S4. XRD patterns of Co-ZIF-67 and P-AT@Co-ZIF-67 (a), Co_9S_8-NSC (b), Co-C (c), Mo_2C-NSC (d), and NSC (e).

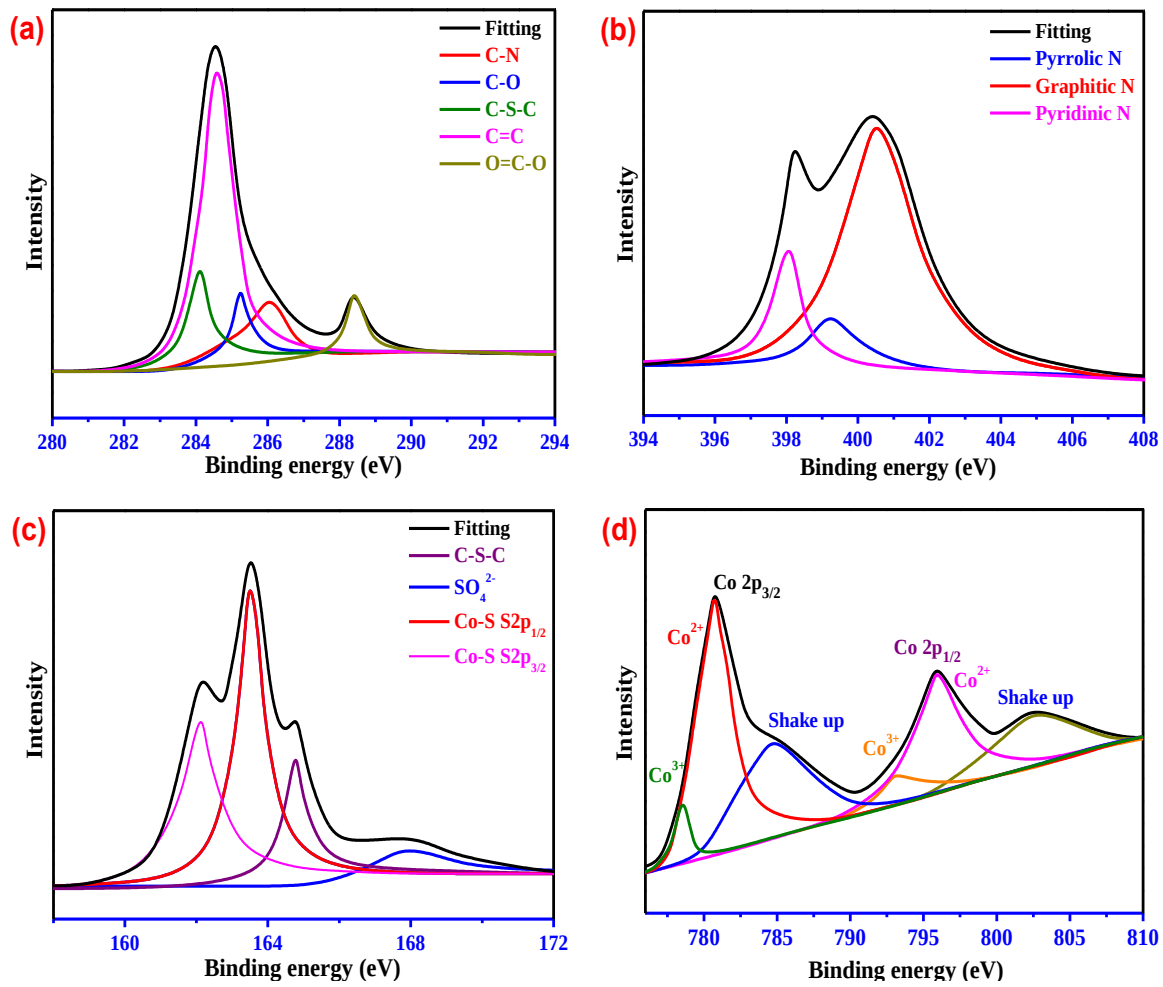

Figure S5. (a) C 1s spectra, (b) N 1s spectra, (c) S 1s spectra and (d) Co 1s spectra of the Co_9S_8-NSC.

Table S1. The Co, Mo, C, N and S elements content determined from XPS spectra of Co_9S_8-NSC@Mo_2C, Mo_2C-NSC and Co_9S_8-NSC.

Elements	Co content (at%)	Mo content (at%)	N content (at%)	S content (at%)
Co_9S_8-NSC @Mo_2C	14.3	12.5	3.6	7.2
Mo_2C-NSC	/	19.6	6.7	10.6
Co_9S_8-NSC	19.5	/	6.3	9.7

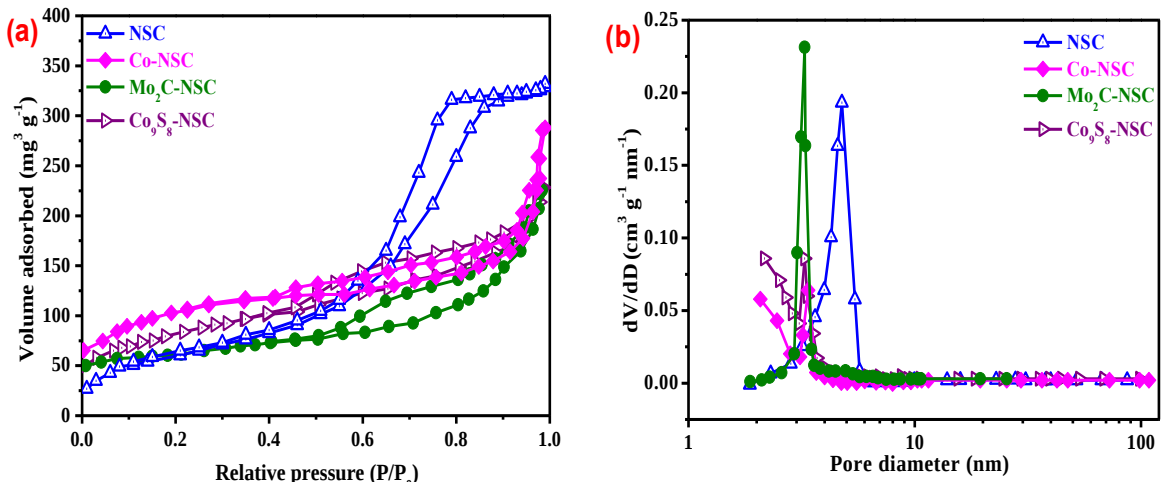

Figure S6. (a) N_2 adsorption/desorption isotherms of NSC, Mo_2C-NSC, Co-NSC, and Co_9S_8-NSC at 77 K and (b) the corresponding pore size distribution from the desorption curve.

Table S2. Comparison of HER activity data for different catalysts.

Catalysts	Electrolyte	Current density ($mV\ cm^{-2}$)	Overpotential (mV)	Tafel slop ($mV\ dec^{-1}$)	References
Amorphous MoS_3	0.5 M H_2SO_4	10	195	60	S2
Cu_3P NW/CF	0.5 M H_2SO_4	10	143	67	S3
Ni_5P_4-Ni_2P/NF	0.5 M H_2SO_4	10	120	79	S4
MoP	0.5 M H_2SO_4	10	135	54	S5
NC/CuCo/$CuCoO_x$	0.5M H_2SO_4	10	112	55	S6
NS-doped Mo_2C	0.5 M H_2SO_4	10	86	47	S7
MoxC-Ni@NCV	0.5 M H_2SO_4	10	75	45	S8
Co_9S_8/NC@MoS_2	0.5 M H_2SO_4	10	117	68.8	S9
CoP nanowire	1.0 M KOH	10	209	129	S10
NiCo/$NiCoO_x$	1.0 M KOH	10	155	35	S11
$NiCo_2O_4$/NF	1.0 M KOH	10	164	107	S12
NiCoP/rGO	1.0 M KOH	10	209	124	S13
Ni-Co-P	1.0 M KOH	10	150	60	S14
N@$MoPC_x$-800	1.0 M KOH	10	139	86.6	S15
Co_9S_8-NSC@Mo_2C	0.5 M H_2SO_4	10	74	69.3	This work
Co_9S_8-NSC@Mo_2C	1.0 M KOH	10	89	86.7	This work

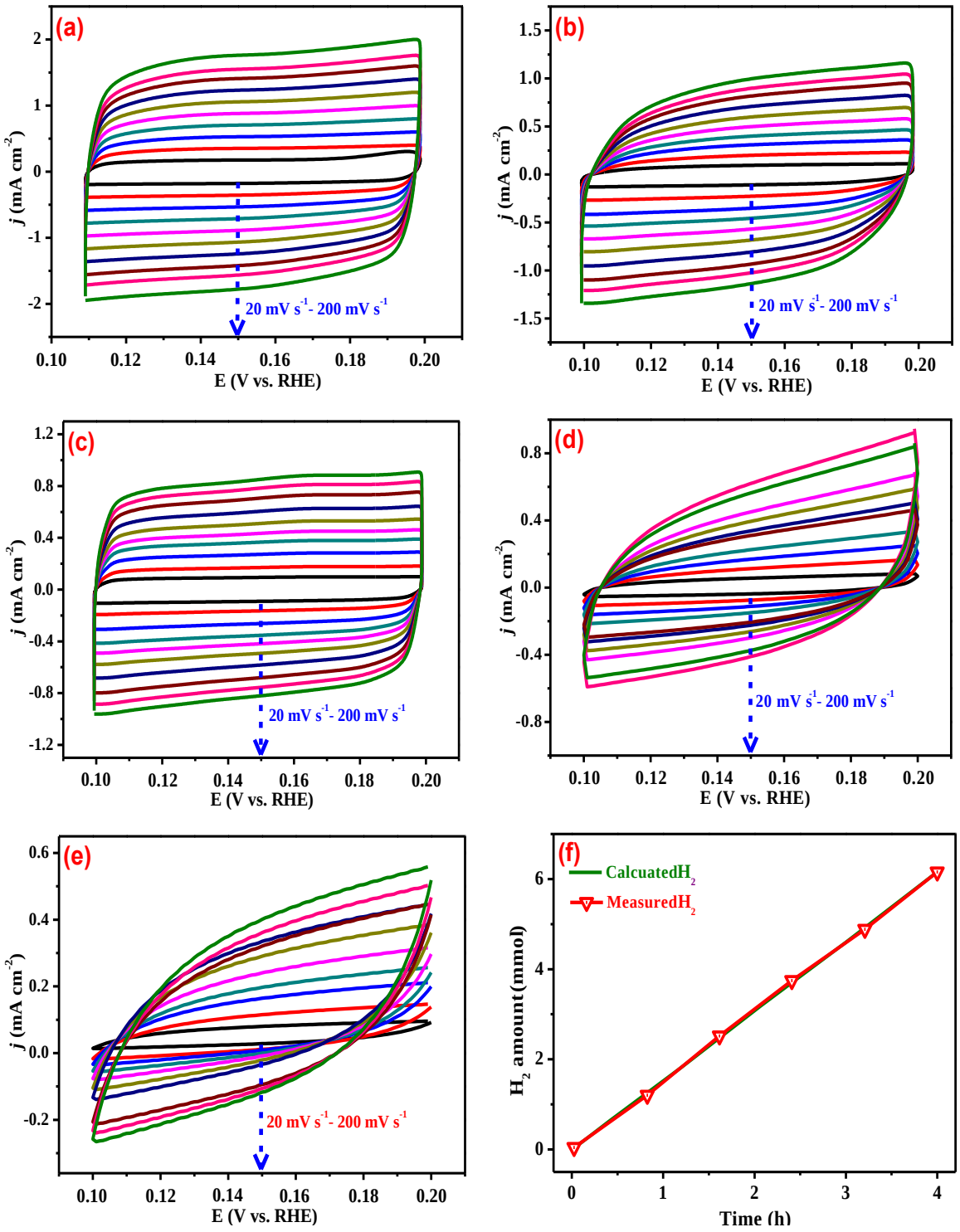

Figure S7. The CV voltammetry curves for the Co_9S_8-NSC@Mo_2C (a), Co_9S_8-NSC (b), Mo_2C-NSC (c), Co-NSC (d) and NSC (e) in 0.5 M H_2SO_4 solution at different potential scanning rates; (f) The amount curves of theoretical and experimental H_2 versus time of the Co_9S_8-NSC@Mo_2C at 150 mV vs. RHE in 0.5 M H_2SO_4 solution.

Cyclic voltammetry (CV) was performed to calculate the electrochemical double layer capacitance (C_{dl}) in nonfaradaic region from 0.1 to 0.2 V vs. RHE at a various scan rates

(20-200 mV s^{-1}). The C_{dl} was determined by plotting $\triangle j$ ($\triangle j = j_{anodic} - j_{cathodic}$ at 150 mV vs. RHE) against the scan rate.

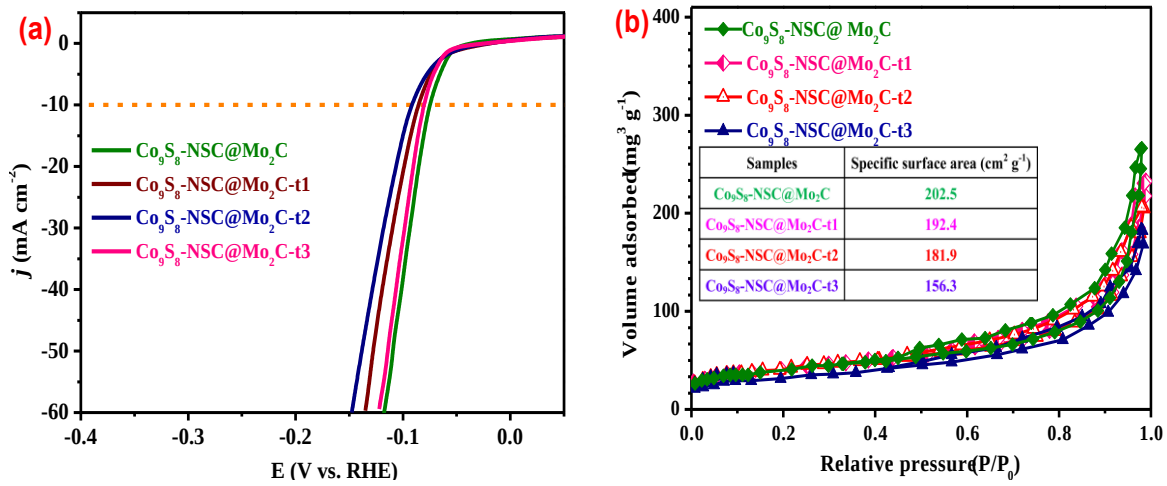

Figure S8. (a) HER polarization curves of Co_9S_8-NSC@Mo_2C, Co_9S_8-NSC@Mo_2C-t1, Co_9S_8-NSC@Mo_2C-t2, and Co_9S_8-NSC@Mo_2C-t3 in 0.5 M H_2SO_4 solution at a scan rate of 5 mV s^{-1}. (b) N_2 adsorption/desorption isotherms of Co_9S_8-NSC@Mo_2C, Co_9S_8-NSC@Mo_2C-t1, Co_9S_8-NSC@Mo_2C-t2, and Co_9S_8-NSC@Mo_2C-t3 at 77 K.

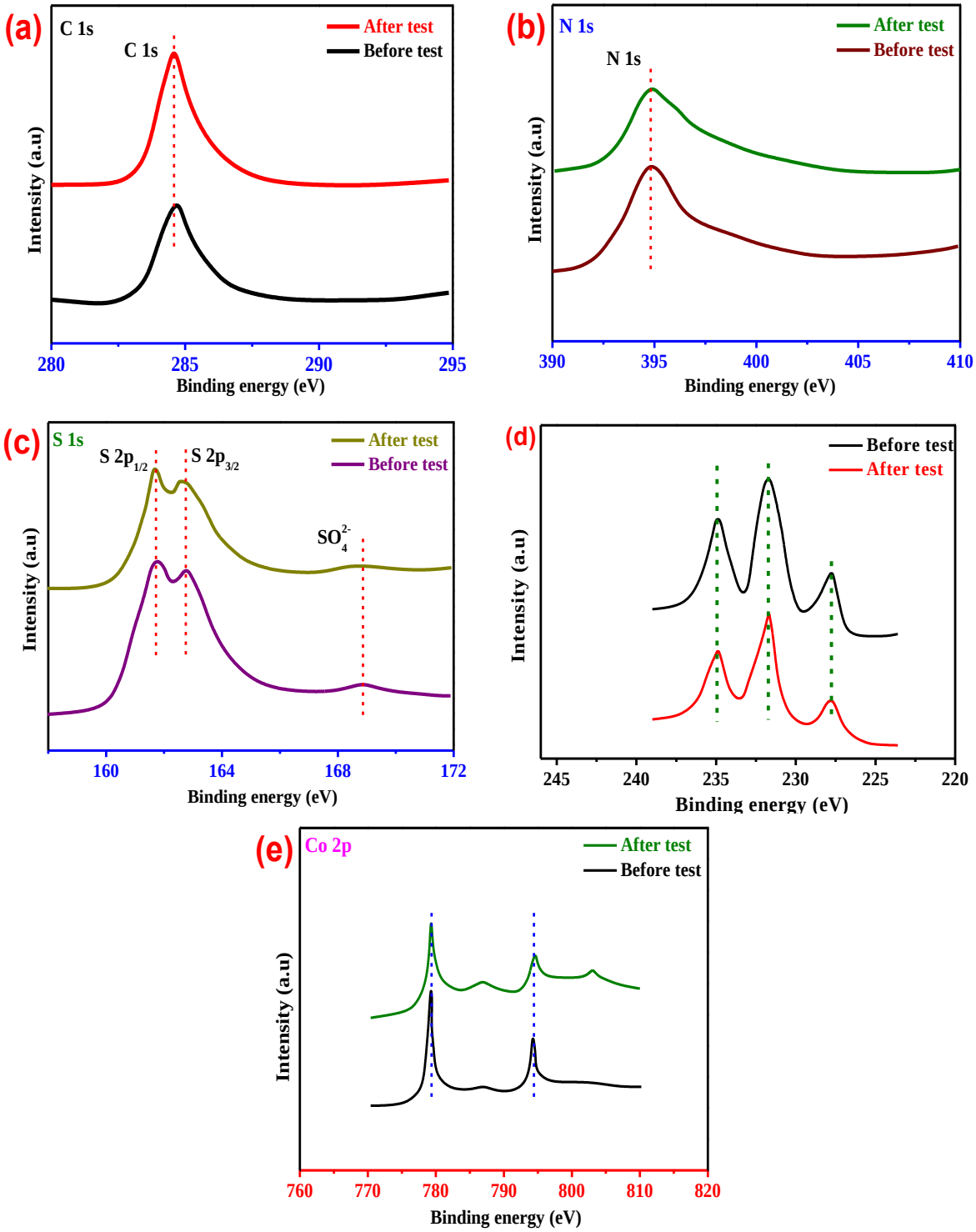

Figure S9. XPS spectrum of the Co_9S_8-NSC@Mo_2C electrocatalyst before and after 20 h durability measurements in 0.5 M H_2SO_4 solution: C 1s spectra (a), N 1s spectra (b), S 2p spectra (c), Mo 3d spectra (d), and Co 2p spectra (e).

Table S3. Determination of the compositions of Co, Mo, N, and S elements in Co_9S_8-NSC@Mo_2C and the 0.5 M H_2SO_4 solution before and after 20 h durability measurements by the ICP-AES (concentration, μg L^{-1}).

Samples	Co	Mo	N	S
H_2SO_4 solution (before)	10.2	11.5	23.3	27.8
H_2SO_4 solution (after)	15.7	14.4	32.6	33.2
Co_9S_8-NSC@Mo_2C (before)	1623.2	1412.8	406.5	772.4
Co_9S_8-NSC@Mo_2C (after)	1612.1	1409.7	396.9	757.8

Inductively coupled plasma-atomic emission spectrometry (ICP-AES) was carried out to demonstrate the chemical stability of Co_9S_8-NSC@Mo_2C hybrid catalyst. The results are displayed in **Table S3**. It is worth noting that the concentrations of Co, Mo, N, and S elements in the Co_9S_8-NSC@Mo_2C electrodes and electrolytes have no obvious changes before and after HER measurements. Therefore, Co_9S_8-NSC@Mo_2C shows good chemical stability during HER reactions.

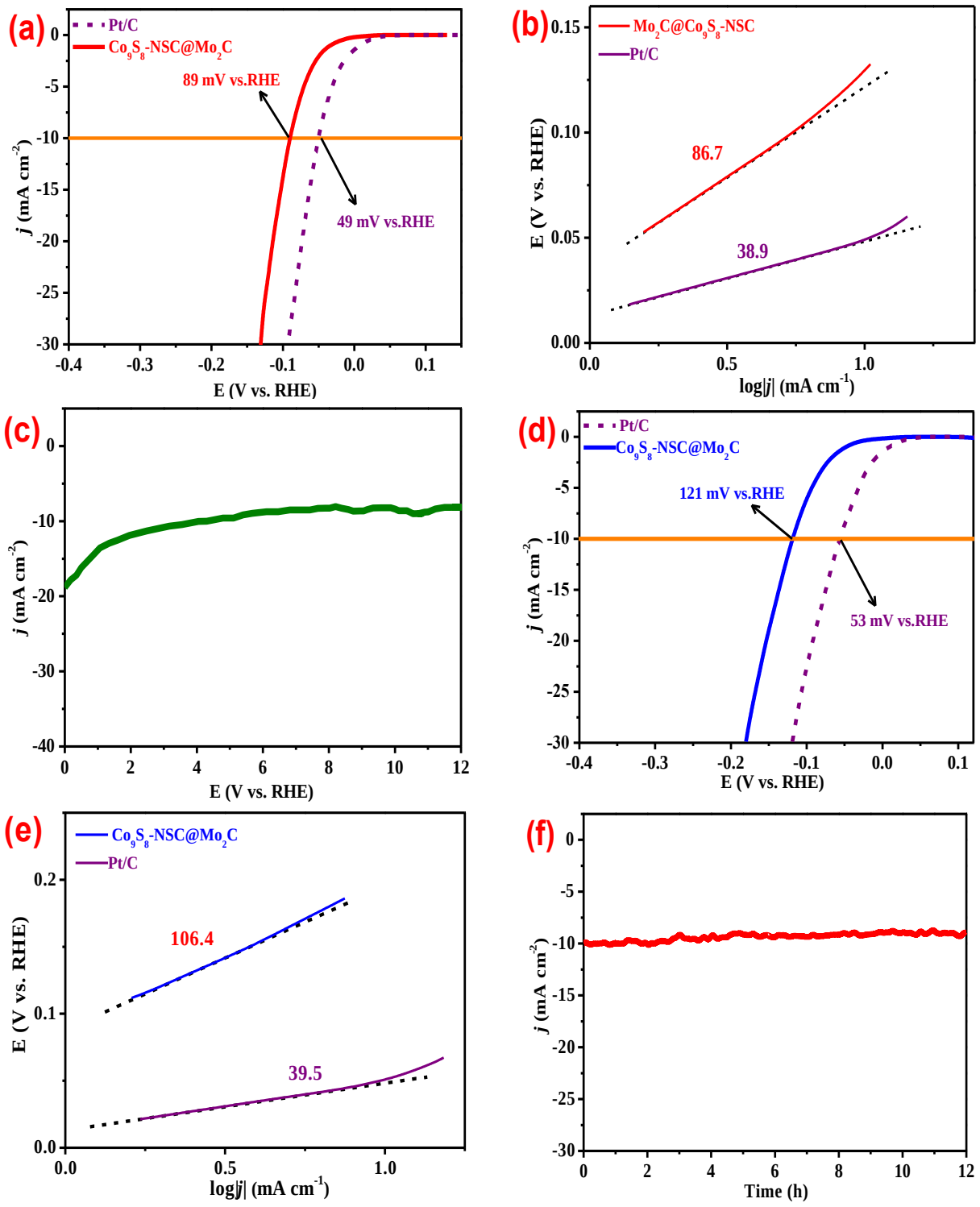

Figure S10. HER polarization curves (a) and corresponding Tafel slops (b) of the Co_9S_8-NSC@Mo_2C and Pt/C in 1.0 M KOH solution at a scan rate of 5 mV s^{-1}. Time-depend current density curve (c) for the Co_9S_8-NSC@Mo_2C in 1.0 M KOH solution at an overpential of 89 mV vs. RHE for 12 h. HER polarization curves (d) and corresponding Tafel slops (e) of the Co_9S_8-NSC@Mo_2C and Pt/C in 1.0 M PBS solution at a scan rate of 5 mV s^{-1}. Time-depend current density curve (f) for the Co_9S_8-NSC@Mo_2C

in 1.0 M PBS solution at an overpential of 121 mV vs. RHE for 12 h.

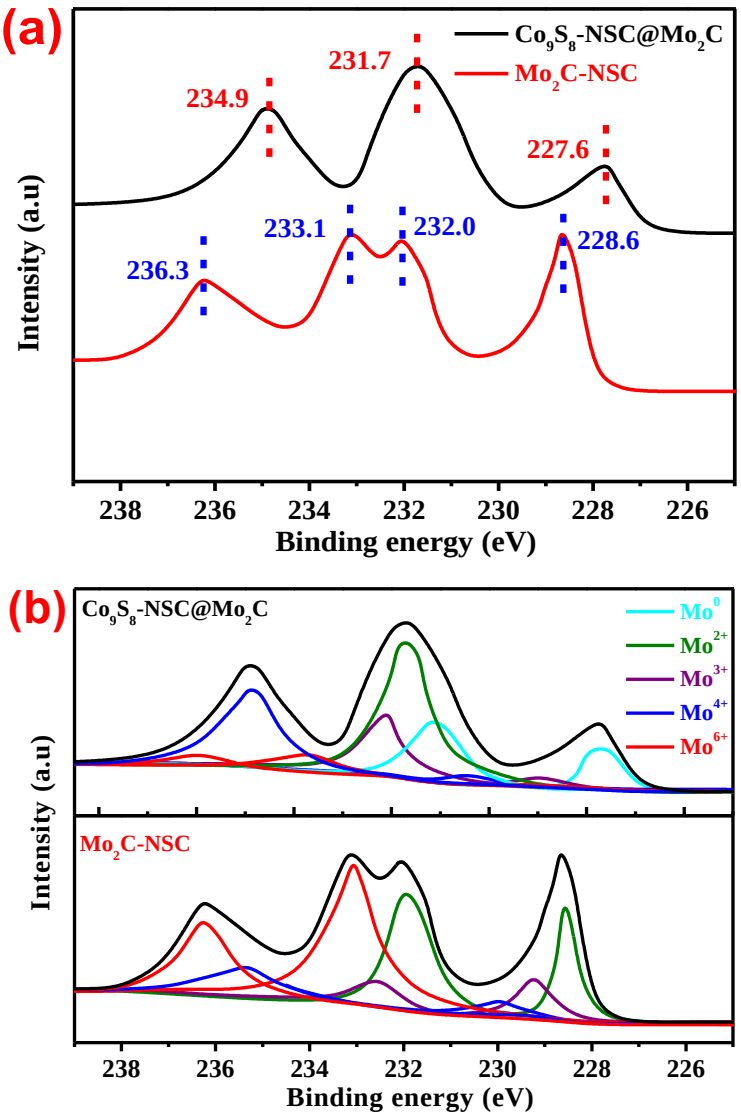

Figure S11. (a) Mo 3d XPS spectra and (b) high-resolution Mo 3d XPS spectra for Co_9S_8-NSC@Mo_2C and Mo_2C-NSC.

It is worth noting that the XPS results show the N and S elements contents in the NSC, Mo_2C-NSC, and Co_9S_8-NSC are much higher than that in Co_9S_8-NSC@Mo_2C (**Table S1**). Besides, the specific surface area of NSC, Mo_2C-NSC, and Co_9S_8-NSC are also higher than that of Co_9S_8-NSC@Mo_2C (**Figure S6**). However, the HER activity of NSC, Mo_2C-NSC, and Co_9S_8-NSC is much lower than that of Co_9S_8-NSC@Mo_2C, thus it is reasonably inferred that the heteroatom doping and specific surface area are not main reasons for the enhanced activity of Co_9S_8-NSC@Mo_2C.

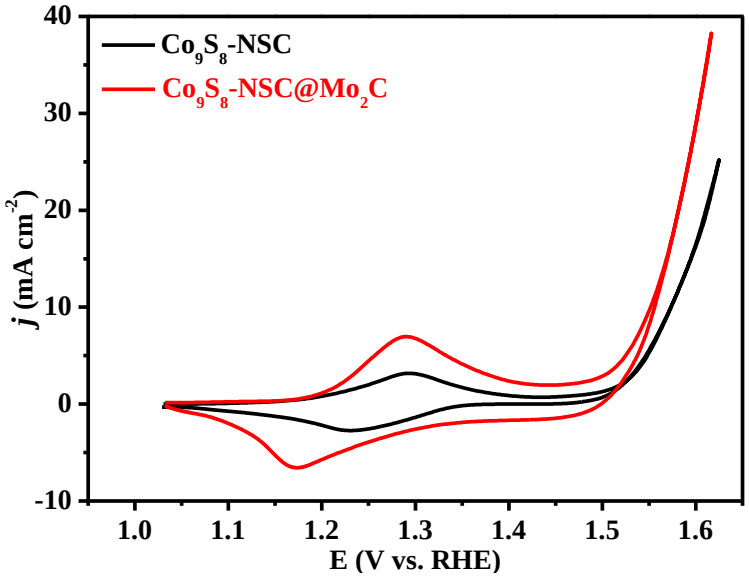

Figure S12. Cyclic voltammograms of the Co_9S_8-NSC@Mo_2C and Co_9S_8-NSC catalysts at a scan rate of 10 mV s^{-1} with iR corrections. The loading of catalyst is 0.71 mg cm^{-2} supported on GC electrode.

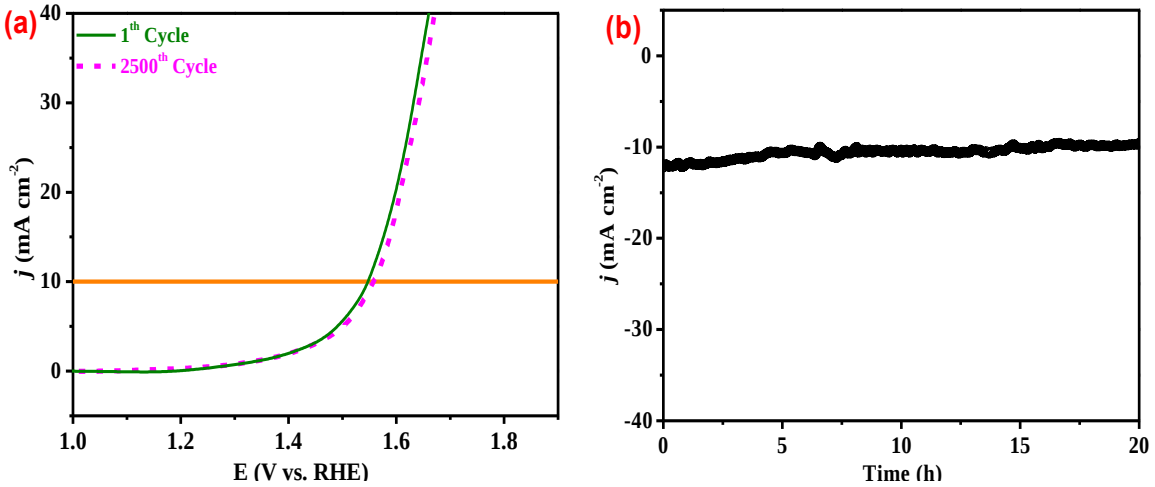

Figure S13. OER polarization curves (a) for the Co_9S_8-NSC@Mo_2C before and after 2500 CV cycles with a potential range from 1.0 to 1.8 V vs. RHE in 1.0 M KOH solution. The current-time curves (b) of the Co_9S_8-NSC@Mo_2C in 1.0 M KOH solution at an overpotential of 1.53 V vs. RHE for 20 h.

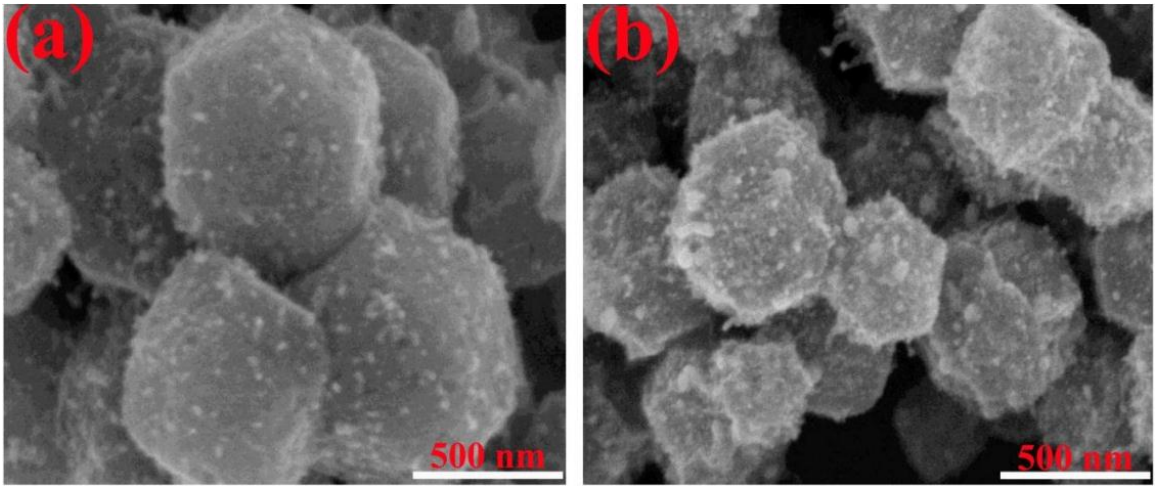

Figure S14. SEM images of Co_9S_8-NSC@Mo_2C composite catalyst before (a) and after (b) 20 h in 1.0 M KOH solution.

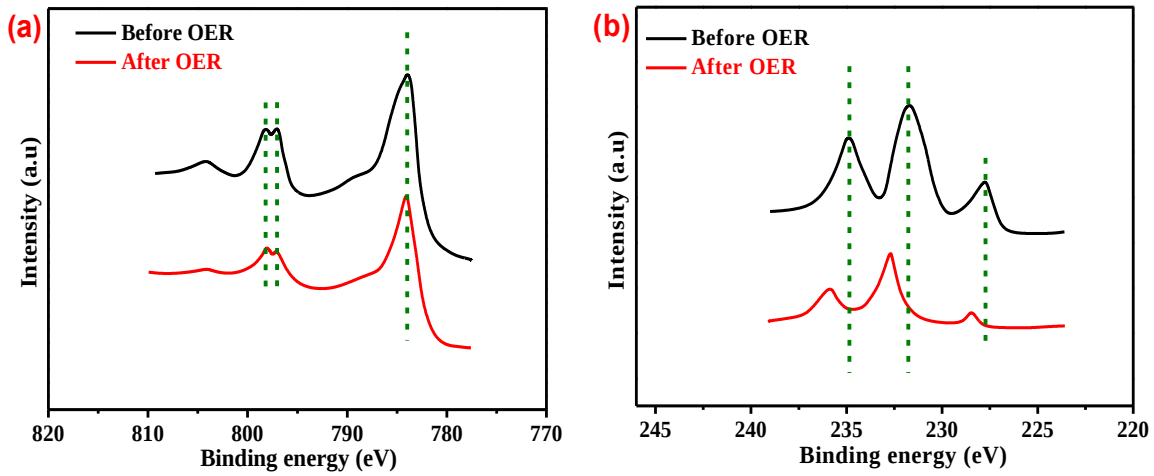

Figure S15. XPS spectrum of the Co_9S_8-NSC@Mo_2C electrocatalyst before and after 20 h durability measurements in 1.0 M KOH solution: (a) Co 2p spectra and (b) Mo 3d spectra.

Table S4. Comparison of OER activity data for different catalysts.

Catalysts	Electrolyte	Current density (mV cm^{-2})	Overpotential (mV)	Tafel slop (mV dec^{-1})	References
$NiCo/NiCoO_x$	1.0 M KOH	10	361	80	S11
NiMo HNRs/Ti mesh	1.0 M KOH	10	310	47	S16
$Co_{0.5}Fe_{0.5}S$@N-MC	1.0 M KOH	10	410	67	S17
$Co_3O_4/NiCo_2O_4$ DSNCs	1.0 M KOH	10	340	88	S18
Ni-Co binary oxides	0.1 M KOH	10	325	39	S19
Co_9S_8@NOSC-900	1.0 M KOH	10	340	68	S20
$CoMoO_4$ flowers	1.0 M KOH	10	400	83	S21
$Fe_3O_4@Co_9S_8$/rGO-2	1.0 M KOH	10	340	54.5	S22
NC/CuCo/CuCo Ox	1.0 M KOH	10	198	88	S6
Co_3O_4@C-MWCNTs	1.0 M KOH	10	320	62	S23
Co_9S_8-NSC@Mo_2C	1.0 M KOH	10	293	59.7	This work

REFERENCES

(S1) Solmaz, R.; Kardaş, G. Electrochemical Synthesis and Characterization of Poly-2-aminothiazole. *Prog. Org. Coat.* **2009,** 64, 81-88.

(S2) Benck, J. D.; Chen, Z.; Kuritzky, L. Y.; Forman, A. J.; Jaramillo, T. F. Amorphous Molybdenum Sulfide Catalysts for Electrochemical Hydrogen Production: Insights into the Origin of their Catalytic Activity. *ACS Catal.* **2012,** 2, 1916-1923.

(S3)Tian, J.; Liu, Q.; Cheng, N.; Asiri, A. M.; Sun, X. Self-Supported Cu_3P Nanowire Arrays as an Integrated High-Performance Three-Dimensional Cathode for Generating Hydrogen from Water. *Angew. Chem. Int. Ed.* **2014,** 53, 9577-9581.

(S4) Tang, C.; Cheng, N.; Pu, Z.; Xing, W.; Sun, X. NiSe Nanowire Film Supported on Nickel Foam: An Efficient and Stable 3D Bifunctional Electrode for Full Water Splitting. *Angew. Chem. Int. Ed.* **2015,** 127, 9483-9487.

(S5) Xiao, P.; Sk, M. A.; Thia, L.; Ge, X.; Lim, R. J.; Wang, J.-Y.; Lim, K. H.; Wang, X. Molybdenum Phosphide as an Efficient Electrocatalyst for the Hydrogen Evolution Reaction. *Energy Environ. Sci.* **2014,** 7, 2624-2629.

(S6) Hou, J.; Sun, Y.; Wu, Y.; Cao, S.; Sun, L. Promoting Active Sites in Core–Shell Nanowire Array as Mott–Schottky Electrocatalysts for Efficient and Stable Overall Water Splitting. *Adv. Funct. Mater.* **2017**, 1704447.

(S7) Ang, H.; Tan, H. T.; Luo, Z. M.; Zhang, Y.; Guo, Y. Y.; Guo, G.; Zhang, H.; Yan, Q. Hydrophilic Nitrogen and Sulfur Co-doped Molybdenum Carbide Nanosheets for Electrochemical Hydrogen Evolution. *Small.* **2015,** 11, 6278-6284.

(S8) Wang, S.; Wang, J.; Zhu, M.; Bao, X.; Xiao, B.; Su, D.; Li, H.; Wang, Y. Molybdenum-Carbide-Modified Nitrogen-Doped Carbon Vesicle Encapsulating Nickel Nanoparticles: A Highly Efficient, Low-Cost Catalyst for Hydrogen Evolution Reaction. *J. Am.Chem. Soc.* **2015,** 137, 15753-15759.

(S9) Li, H.; Qian, X.; Xu, C.; Huang, S.; Zhu, C.; Jiang, X.; Shao, L.; Hou, L. Hierarchical Porous Co_9S_8/Nitrogen-Doped Carbon@MoS_2 Polyhedrons as pH Universal Electrocatalysts for Highly Efficient Hydrogen Evolution Reaction. *ACS Appl. Mater. Interfaces.* **2017,** 9, 28394-28405.

(S10) Tian, J.; Liu, Q.; Asiri, A. M.; Sun, X. Self-Supported Nanoporous Cobalt Phosphide Nanowire Arrays: An Efficient 3D Hydrogen-Evolving Cathode over the Wide Range of pH 0–14. *J. Am. Chem. Soc.* **2014,** 136, 7587-7590.

(S11) Yan, X.; Li, K.; Lyu, L.; Song, F.; He, J.; Niu, D.; Liu, L.; Hu, X.; Chen, X. From Water Oxidation to Reduction: Transformation from $Nix Co_3 – x O_4$ Nanowires to NiCo/NiCoOx Heterostructures. *ACS Appl. Mater. Interfaces.* **2016,** 8, 3208-3214.

(S12) Xiao, C.; Li, Y.; Lu, X.; Zhao, C. Bifunctional Porous $NiFe/NiCo_2O_4$/Ni Foam Electrodes with Triple Hierarchy and Double Synergies for Efficient Whole Cell Water Splitting. *Adv. Funct. Mater.* **2016,** 26, 3515-3523.

(S13) Li, J.; Yan, M.; Zhou, X.; Huang, Z.-Q.; Xia, Z.; Chang, C.-R.; Ma, Y.; Qu, Y. Mechanistic Insights on Ternary $Ni_2 − x Co_x P$ for Hydrogen Evolution and Their Hybrids with Graphene as Highly Efficient and Robust Catalysts for Overall Water Splitting. *Adv. Funct. Mater.* **2016,** 26, 6785-6796.

(S14) Feng, Y.; Yu, X.-Y.; Paik, U. Nickel Cobalt Phosphides Quasi-Hollow Nanocubes as an Efficient Electrocatalyst for Hydrogen Evolution in Alkaline Solution. *Chem. Commun.* **2016,** 52, 1633-1636.

(S15) Huang, Y.; Ge, J.; Hu, J.; Zhang, J.; Hao, J.; Wei, Y. Nitrogen-Doped Porous Molybdenum Carbide and Phosphide Hybrids on a Carbon Matrix as Highly Effective Electrocatalysts for the Hydrogen Evolution Reaction. *Adv. Energy Mater.* **2017,** 1701601.

(S16) Tian, J.; Cheng, N.; Liu, Q.; Sun, X.; He, Y.; Asiri, A. M. Self-supported NiMo Hollow Nanorod Array: an Efficient 3D Bifunctional Catalytic Electrode for Overall Water Splitting. *J. Mater. Chem. A.* **2015,** 3, 20056-20059.

(S17) Shen, M.; Ruan, C.; Chen, Y.; Jiang, C.; Ai, K.; Lu, L. Covalent Entrapment of Cobalt–Iron Sulfides in N-Doped Mesoporous Carbon: Extraordinary Bifunctional Electrocatalysts for Oxygen Reduction and Evolution Reactions. *ACS Appl. Mater. Interfaces.* **2015,** 7, 1207-1218.

(S18) Hu, H.; Guan, B.; Xia, B.; Lou, X. W. Designed Formation of Co3O4/NiCo2O4 Double-Shelled Nanocages with Enhanced Pseudocapacitive and Electrocatalytic Properties. *J. Am Chem. Soc.* **2015,** 137, 5590-5595.

(S19) Zhao, A.; Masa, J.; Xia, W.; Maljusch, A.; Willinger, M.-G.; Clavel, G.; Xie, K.; Schlögl, R.; Schuhmann, W.; Muhler, M. Spinel Mn–Co Oxide in N-Doped Carbon Nanotubes as a Bifunctional Electrocatalyst Synthesized by Oxidative Cutting. *J. Am. Chem. Soc.* **2014,** 136, 7551-7554.

(S20) Huang, S.; Meng, Y.; He, S.; Goswami, A.; Wu, Q.; Li, J.; Tong, S.; Asefa, T.; Wu, M. N-, O-, and S-Tridoped Carbon-Encapsulated Co_9S_8 Nanomaterials: Efficient Bifunctional Electrocatalysts for Overall Water Splitting. *Adv. Funct. Mater.* **2017,** 27, 1606585.

(S21) Yu, M. Q.; Jiang, L. X.; Yang, H. G. Ultrathin Nanosheets Constructed $CoMoO_4$ Porous Flowers with High Activity for Electrocatalytic Oxygen Evolution. *Chem. Commun.* **2015,** 51, 14361-14364.

(S22) Yang, J.; Zhu, G.; Liu, Y.; Xia, J.; Ji, Z.; Shen, X.; Wu, S. Fe_3O_4-Decorated Co9S8 Nanoparticles In Situ Grown on Reduced Graphene Oxide: A New and Efficient Electrocatalyst for Oxygen Evolution Reaction. *Adv. Funct. Mater.* **2016,** 26, 4712-4721.

(S23) Li, X.; Fang, Y.; Lin, X.; Tian, M.; An, X.; Fu, Y.; Li, R.; Jin, J.; Ma, J. MOF Derived Co_3O_4 Nanoparticles Embedded in N-Doped Mesoporous Carbon Layer/MWCNT Hybrids: Extraordinary Bi-Functional Electrocatalysts for OER and ORR. *J. Mater. Chem. A.* **2015,** 3, 17392-17402.